NANO LETTERS

pubs.acs.org/NanoLett
Letter

Observation of Near-Field Thermal Radiation between Coplanar Nanodevices with Subwavelength Dimensions

Xiao Luo,‡ Hakan Salihoglu,‡ Zexiao Wang,‡ Zhuo Li,‡ Hyeonggyun Kim, Xiu Liu, Jiayu Li, Bowen Yu, Shen Du, and Sheng Shen*

Cite This: *Nano Lett.* 2024, 24, 1502−1509

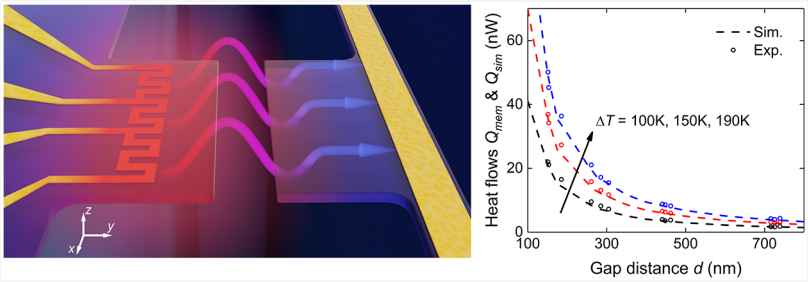

ABSTRACT: With the continuous advancement of nanotechnology, nanodevices have become crucial components in computing, sensing, and energy conversion applications. The structures of nanodevices typically possess subwavelength dimensions and separations, which pose significant challenges for understanding energy transport phenomena in nanodevices. Here, on the basis of a judiciously designed thermal photonic nanodevice, we report the first measurement of near-field energy transport between two coplanar subwavelength structures over temperature bias up to ∼190 K. Our experimental results demonstrate a 20-fold enhancement in energy transfer beyond blackbody radiation. In contrast with the well-established near-field interactions between two semi-infinite bodies, the subwavelength confinements in nanodevices lead to increased polariton scattering and reduction of supporting photonic modes and, therefore, a lower energy flow at a given separation. Our work unveils exciting opportunities for the rational design of nanodevices, particularly for coplanar near-field energy transport, with important implications for the development of efficient nanodevices for energy harvesting and thermal management.

KEYWORDS: *coplanar nanodevices, subwavelength dimensions, near-field thermal radiation, subwavelength confinements, thermal photonic nanodevices*

Nanodevices play a vital role in a broad range of emerging technologies, including quantum computing,[1] nanophotonic biosensors,[2] and widely tunable nanolasers.[3] These devices often consist of active elements with subwavelength dimensions and separations (λ < ∼10 μm at room temperature), which give rise to unusual energy transport paths, such as super-Planckian far-field thermal radiation[4] and quantum fluctuational energy transport, between the subwavelength elements across vacuum separations via Casimir effect.[5−7] Particularly at subwavelength separations, near-field thermal radiation exhibits remarkable energy transport enhancements and exceeds well-established blackbody radiation by orders of magnitude.[8−11] Leveraging such near-field enhancements between nanoscale elements opens up extraordinary applications of nanodevices in thermal management[12,13] and energy harvesting.[14−16] However, the realization of near-field-based thermal nanodevices has remained elusive because of the challenges in fabrication and measurement. Previous experimental near-field studies[11,17−35] have extensively focused on the near-field radiation involving macroscopic structures much larger than wavelengths. Among these studies, near-field thermal signal would be buried within heat conduction for devices based on micropillars/posts/particles support[17−25] when the dimensions of the emitter and receiver are comparable with the supporting structures. Devices based on nanopositioning platforms[11,26−35] face the challenge of aligning the subwavelength structures. On-chip devices[8,36] can circumvent these abovementioned issues but face the difficulty of realizing coplanarity for subwavelength structures due to deflection.[4] Besides, subwavelength structures also indicate a smaller heat exchange area and, thus, a smaller thermal signal. So far, experiments reporting radiation thermal conductance below 1 nW/K are very limited.[9] Current knowledge of near-

Received: September 29, 2023
Revised: January 1, 2024
Accepted: January 22, 2024
Published: January 26, 2024

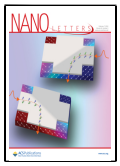

https://doi.org/10.1021/acs.nanolett.3c03748
Nano Lett. 2024, 24, 1502−1509

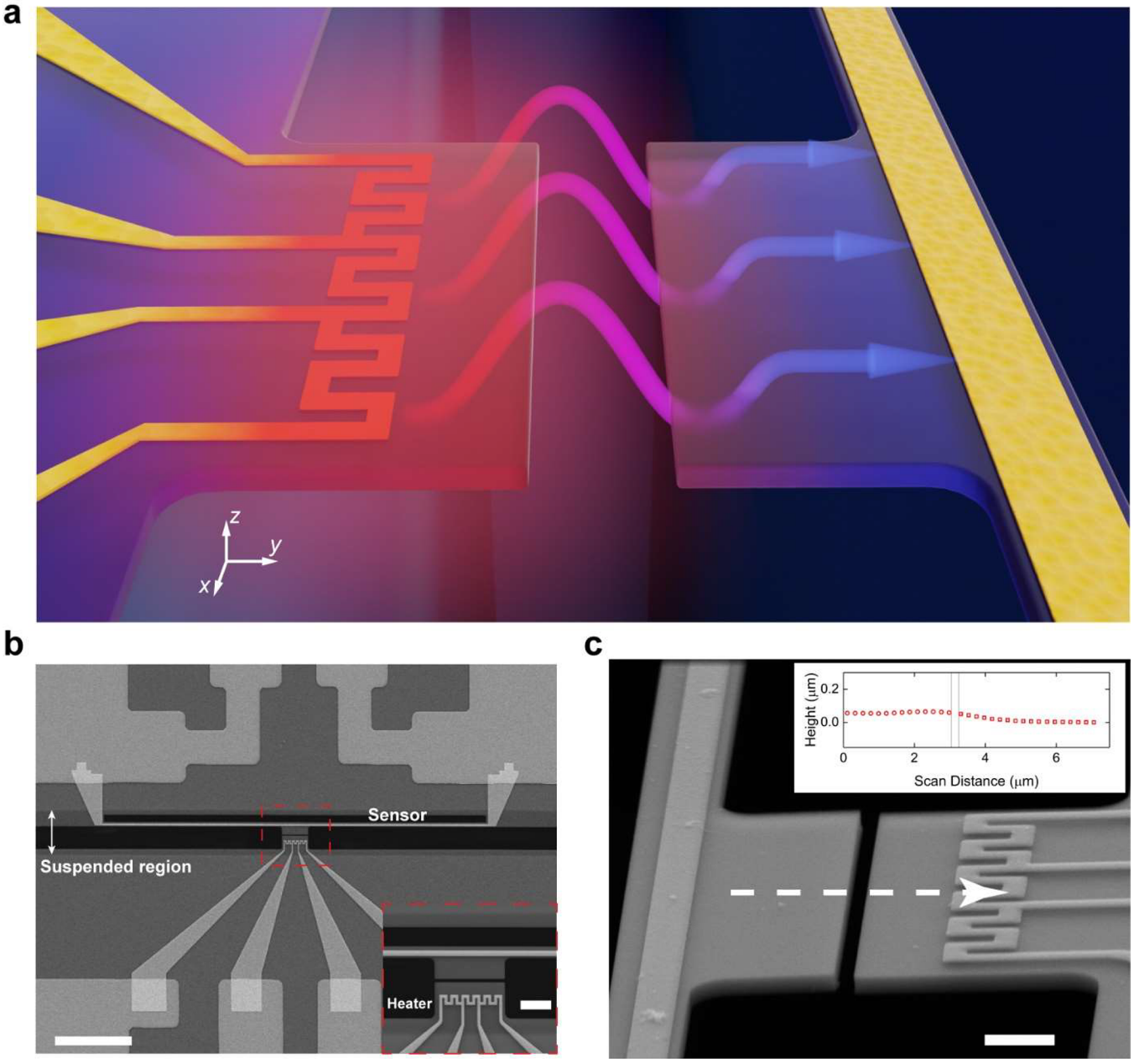

Figure 1. Nanodevice-enabled near-field thermal radiation between parallel subwavelength membranes. (a) Schematic of a near-field thermal nanodevice. The extruded emitting membrane (left) is heated up by platinum serpentine heater, while the extruded absorbing membrane (right) absorbs the near-field radiation with a temperature rise monitored by the platinum resistance thermometer. (b) Top-view SEM images of the measurement nanodevice. Scale bar: 25 μm. The inset shows the zoomed-in SEM image. Scale bar: 3 μm. To physically isolate the emitting and absorbing membranes and, thus, exclude heat conduction, the heater and sensor structures are suspended by etching the underlying silicon substrate, as shown by the suspended region. The width of the suspended region is confined within 15 μm to maintain the coplanarity of the two membranes. (c) Tilted SEM image taken from 70° altitude angle. Scale bar: 1 μm. The inset shows the measured profile along the dashed arrow indicating a height difference of ∼50 nm.

field thermal radiation heavily relies on fluctuational electrodynamic framework derived on the basis of semi-infinite bodies[37,38] or multilayered structures,[39−41] which assume infinite dimensions and neglect geometrical constraints of the surfaces. In contrast, subwavelength structures enable distinct energy transport physics in the near field where lateral confinements[42] may support new guided surface modes or filter certain radiation modes.

To unlock the potential of near-field thermal radiation in nanodevices, here, we employ custom-built coplanar nanodevices that are designed to measure the near-field thermal radiation between two coplanar subwavelength membranes with nanofabricated gaps ranging from ∼150 to ∼750 nm. By integrating them with suspended platinum resistive heating and thermometry, our coplanar nanodevices allow for precise detection of near-field radiative heat transfer between subwavelength surfaces over a wide range of temperature differences up to ∼190 K. Because of the mode suppression from subwavelength confinement, the measured near-field heat flows are observed to be smaller than the analytical predictions derived for the well-known semi-infinite bodies.

https://doi.org/10.1021/acs.nanolett.3c03748
Nano Lett. 2024, 24, 1502−1509

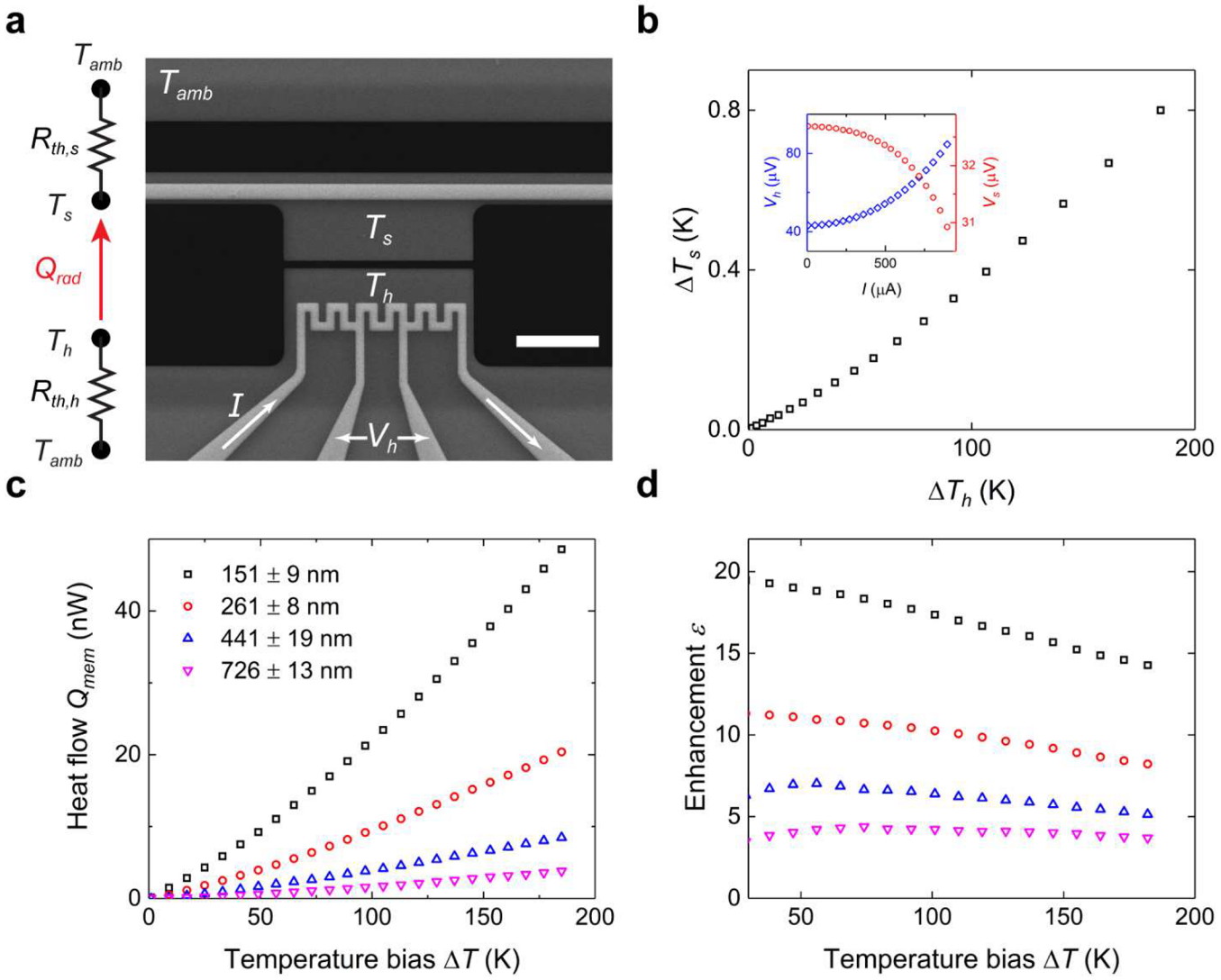

Figure 2. Near-field measurement setup and experimental results. (a) Measurement setup and corresponding thermal circuit. The absorbed radiation heat flow Q_{rad} is dissipated to the ambient via heat conduction, which induces a temperature rise of the sensor. Scale bar: 3 μm. (b) Measured temperature increase of the absorbing membrane and corresponding temperature rise of the emitting membrane. The temperature increases of the emitting ΔT_h and absorbing ΔT_s membranes are monitored by the four-probe voltage V_h and gap voltage of the Wheatstone bridge V_s, respectively. The inset shows the measured voltages as a function of heating current, I, for a near-field nanodevice with a 151 nm separation. (c) Measured radiation heat flow as a function of temperature bias of different gap distances. For the maximum temperature bias considered, the heat flow increases from ∼4 nW to ∼50 nW as the gap distance decreases from 726 to 151 nm, corresponding to maximum radiation heat conductance of ∼0.26 nW/K. (d) Heat flow enhancement ratio compared with blackbody radiation calculated by $Q_{bb} = \sigma A F_{12}(T_h^4 - T_s^4)$.

As depicted in Figure 1a, our coplanar nanodevice comprises two suspended coplanar silicon nitride membranes with lateral dimensions of 300 nm in thickness (t) and 7 μm in length (l). The emitting and absorbing membranes are extruded from their corresponding bases by widths (w) of 3.5 and 2 μm, respectively. A platinum serpentine heater fabricated on the emitting membrane is used to increase the membrane temperature, whereas a platinum thermometry sensor on the absorbing membrane measures the temperature rise induced by near-field radiative heat transfer. To avoid the influence of heat conduction, the silicon substrate beneath the silicon nitride membranes is etched to form a suspended region (marked in Figure 1b). On the absorbing membrane, a 100 μm long trench is cut behind the platinum to fabricate a 1D long beam structure as the resistive thermometry sensor for heat flow probing. To investigate the coupled near-field interactions between two subwavelength structures (protruded parts on the emitting and absorbing membranes), we fabricate the coplanar nanodevices with a range of nanoscale separations from ∼150 to ∼750 nm using electron beam lithography. As shown in Figure 1c for the tilted-angle scanning electron microscope (SEM) image of a typical nanodevice, the width of the suspended region is controlled to <15 μm to ensure good coplanarity and minimal relative deflection of the membranes. The height profile measurements with a Zyro noncontact profilometer reveal a height deviation of ∼50 nm across the separation gap (Figure 1c, inset). By designing the serpentine heater, we achieve a uniform temperature profile along the y-axis within the first 2 μm deep region and minimize the temperature increase at the base of the emitting membrane along the x-axis (see the Supporting Information for the simulated temperature profile). We specifically design for a uniform temperature distribution along the first 2 μm from the edge because the near-field radiation is dominated by the first

https://doi.org/10.1021/acs.nanolett.3c03748
Nano Lett. 2024, 24, 1502−1509

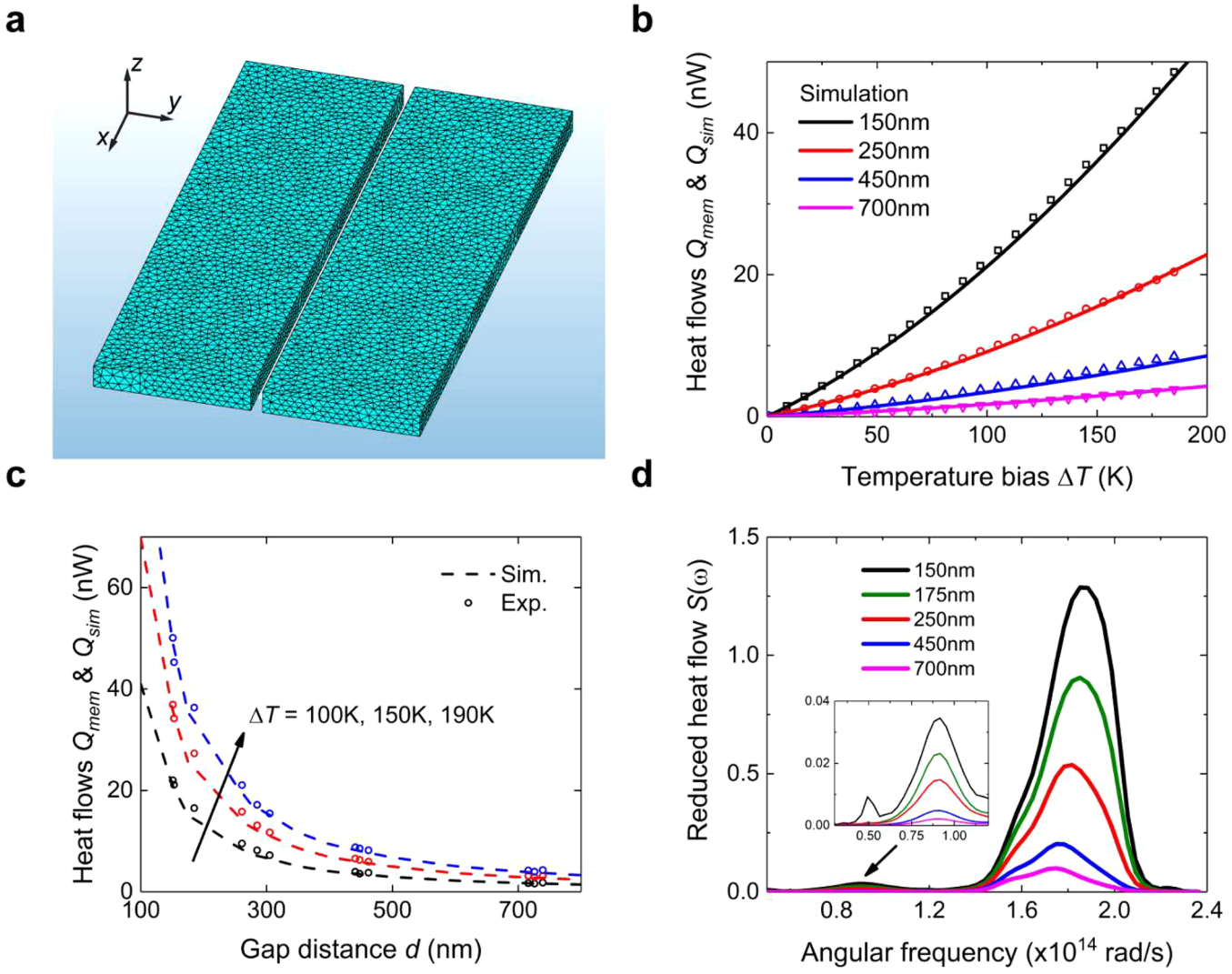

Figure 3. Fluctuational-EM simulation and comparison with measurements. (a) Surface mesh generated for the FSC method. (b) Comparison between the simulated and measured heat flows. The measurements show excellent agreement with the simulations. (c) Comparison between the simulated and measured heat flows as a function of gap distance for the temperature biases of 100, 150, and 190 K, respectively. (d) Reduced heat flow spectra. The inset shows the zoomed-in spectrum in the low frequency range.

~2 μm from the edge (see the Supporting Information). The suspended base efficiently dissipates heat along the y-axis because of the short pathway to the intact silicon wafer (as the heat sink), and the temperature drops to ambient temperature within a short distance, which ensures the minimized thermal emission from the base of the emitting membrane to the absorbing membrane. Meanwhile, we also design reference devices to measure any background radiation absorbed by the sensor beam (see the Supporting Information for reference device design).

Figure 2a illustrates the measurement scheme and the corresponding thermal circuits in our experiments. All measurements are performed under high vacuum (10^{-3} Pa) with an ambient temperature, T_{amb}, maintained at 300 K by a temperature controller. Here, the Si substrate acts as a thermal reservoir because of the very large dimensions (~7 mm long and wide with 500 μm thickness) compared with the nanodevice dimensions and has good thermal contact with the chamber environment maintained at 300 K. Thus, the base temperature of the emitting membrane and the temperatures at both ends of the suspended beam are held at T_{amb}. A DC current I is supplied to the serpentine heater for heating the emitting membrane, and the substrate dissipates the Joule heating with thermal resistance $R_{th,h}$. For our near-field thermal measurement, it is not necessary to calibrate the thermal resistance $R_{th,h}$. The increase of the heater temperature ΔT_h ($\Delta T_h = T_h - T_{amb}$) is monitored by supplying a small sinusoidal current (0.4 μA at the 211 Hz frequency) and measuring the corresponding four-wire voltage change, ΔV_h. To measure the temperature variation of the absorbing membrane ΔT_s ($\Delta T_s = T_s - T_{amb}$), we use a Wheatstone bridge circuit[43] to detect the voltage change across the long platinum thermometry beam sensor, which dissipates heat to both ends of the sensor via heat conduction by a thermal resistance $R_{th,s}$. For the long and thin suspended beam sensor, it is well justified to assume a 1D heat conduction along the sensor beam with the temperatures of its two ends equal to the ambient temperature.[44] With the thermal radiation input on the absorbing membrane, the corresponding temperature profile along the beam sensor results in the voltage change, ΔV_s (see the Supporting Information for the temperature profile along the beam sensor). Figure 2b shows the measured

https://doi.org/10.1021/acs.nanolett.3c03748
Nano Lett. 2024, 24, 1502−1509

ΔT_h and ΔT_s for a 150 nm gap nanodevice, while the inset demonstrates the corresponding readings of ΔV_h and ΔV_s for the supplied heating current. The corresponding thermal radiation, Q_{rad}, is determined by $Q_{rad} = G_s \Delta T_s$, where G_s is the heat conductance of the beam sensor to ambient, and $G_s = 1/R_{th,s}$. To calibrate G_s, we apply the Joule heating $Q_{s,J}$ to the sensor by supplying a DC current with a small sinusoidal current and monitor the corresponding average temperature increase of the sensor $\overline{\Delta T_{s,J}}$ from the four-wire sinusoidal voltage change: $G_s = Q_{s,J}/3\overline{\Delta T_{s,J}}$ using the 1D heat conduction model (see the Supporting Information for derivations). By knowing G_s and reading ΔT_s under a temperature bias ΔT ($\Delta T = \Delta T_h - \Delta T_s$), we measure the thermal radiation heat flow Q_{rad}. This measurement procedure is repeated for all the nanodevices with various separation gaps and reference devices over a range of ~190 K temperature bias ($\Delta T = \Delta T_h - \Delta T_s \approx \Delta T_h$), i.e., 300−490 K absolute temperature of the heater. To determine the near-field thermal radiation between two extruded membranes, Q_{mem}, we deduct the background radiation heat flow measured by the reference device Q_{ref} from the measured heat flow Q_{rad}.

We measure the radiation heat flows Q_{mem} between the extruded membranes in 12 coplanar nanodevices, categorized into four groups on the basis of gap distances. Figure 2c shows the typical Q_{mem} as a function of the temperature bias ΔT from each group of gap distances in which the corresponding gap distances are measured from SEM images (see the Supporting Information for gap distance measurement). Across all of the nanodevices, we observe that the radiation heat flow Q_{mem} increases with an increase in temperature bias. Furthermore, at a given temperature bias, Q_{mem} rises with reduced gap separation because of the near-field effect. For instance, when the maximum temperature bias of 190 K is applied in our experiments, reduction of the gap distance from 726 to 151 nm leads to a significant heat flow increase from ~4 to ~50 nW, and the corresponding radiation thermal conductance G_{mem} increases from ~0.02 to ~0.26 nW/K. This behavior confirms the enhanced near-field thermal radiation between the membranes at smaller gap distances.

To quantify the near-field enhancement of the membranes, we define an enhancement ratio $\varepsilon = Q_{mem}/Q_{bb}$. Here, $Q_{bb} = \sigma A F_{12}(T_h^4 - T_s^4)$ is the radiation heat flow between two blackbodies with the same configuration as the coplanar nanodevice, where σ is the Stefan−Boltzmann constant, A is the exchange surface area, and F_{12} is the view factor between the exchange surfaces. We plot the enhancement ratio ε as a function of the temperature bias in Figure 2d. Interestingly, over the 190 K temperature bias range, we observe that ε decreases as the temperature bias increases, which will be further discussed in the simulated thermal radiation spectrum. As gap distance increases from 151 to 726 nm, the maximum radiation heat flow decreases by 92% (~50 to ~4 nW), while the maximum enhancement ratio (ε) only decreases by 80% (~20 to ~4) because the view factor F_{12} also drops significantly from ~0.6 to ~0.2 (see the Supporting Information for the calculation of view factor). The maximum enhancement ratio that we measured is ~20 at a 30 K temperature bias and ~150 nm gap distance. We notice that the enhancement ratio is less than the 100-fold enhancement reported in the far field with a similar membrane thickness.[4] We believe that such a discrepancy arises because blackbody radiation also depends on gap distance for coplanar membranes. Blackbody radiation is much weaker at a far-field gap distance than that at a near-field gap distance (see the Supporting Information for the calculations and discussions).

To validate our near-field measurements, we conduct fluctuational electromagnetic (fluctuational-EM) simulation using the fluctuational surface current (FSC) method,[45,46] which considers the two coplanar silicon nitride membranes with the design dimensions of 7 μm × 2 μm × 0.3 μm. Figure 3a shows the surface mesh used for the FSC method, on the basis of which the reduced heat flow spectra $S(\omega)$ are calculated. From this, the simulated near-field heat flow Q_{sim} can be determined by

$$Q_{sim} = \int [\Theta(\omega, T_h) - \Theta(\omega, T_s)] S(\omega) d\omega \quad (1)$$

where $\Theta(\omega, T) = \hbar\omega/[\exp(\hbar\omega/k_B T) - 1]$ represents the Planck energy per oscillator at the temperature T. In Figure 3b, we compare the simulation results to the measurements from the four devices in Figure 2c as a function of temperature bias. For all 12 measured devices, we further compare the simulation results with their measured radiation heat flows as a function of gap distance at multiple temperature biases in Figure 3c. In both temperature- and gap-dependent comparisons, the measured heat flows exhibit good agreement with the simulation results for all the measured separation gaps, thus further validating our experimental results. To elaborate on the mechanism of near-field enhancement, we plot the reduced heat flow spectra of different gap distances in Figure 3d. The major peak around 1.8×10^{14} rad/s corresponds to the resonance of surface phonon polaritons supported by the silicon nitride membrane. In Figure 3d, the reduced heat flow dramatically increases with a decreased gap distance, thereby indicating the strong near-field effect. While the resonance frequency of surface phonon polaritons remains fixed with temperature, the radiative thermal energy peak (based on Wien's law) shifts to higher frequencies as temperature increases, which results in Q_{bb} increasing with a rate higher than that of Q_{mem} for the same ΔT. Consequently, the near-field enhancement ε decreases with increasing ΔT values, as shown in Figure 2d.

To elucidate the impact of subwavelength dimensions in near-field radiative heat transfer, we compare our simulation results for the subwavelength surfaces with the analytical predictions based on the near-field heat flux between two semi-infinite bodies. Figure 4a illustrates that the subwavelength surfaces (solid lines) exchange less heat than the semi-infinite bodies (dashed lines) for the same exchange area of $l \times t = 7 \times 0.3$ μm^2. The observed lower heat flow arises from the boundary scattering of surface phonon polaritons due to the presence of the subwavelength structures, in which some scattered waves escape from the gap and do not contribute to the near-field heat transfer.

In Figure 4b, we define and plot a heat flow ratio, $\varphi_{sim} = Q_{sim}/Q_{semi}$ with respect to separation gap within the temperature range of interest, where Q_{semi} is the predicted heat flow, by multiplying the near-field heat flux between two semi-infinite bodies with the same cross section area ($l \times t$). As a comparison, we also introduce the other heat flow ratio, $\varphi_{exp} = Q_{mem}/Q_{semi}$, which shows excellent agreement with φ_{sim} in Figure 4b. At large separations (d > 500 nm), the difference between Q_{sim} (or Q_{exp}) and Q_{semi} is significant (e.g., φ_{sim} = ~0.2 at d = 800 nm). However, as the separation decreases, the heat transfer rate between the subwavelength surfaces increases

https://doi.org/10.1021/acs.nanolett.3c03748
Nano Lett. 2024, 24, 1502−1509

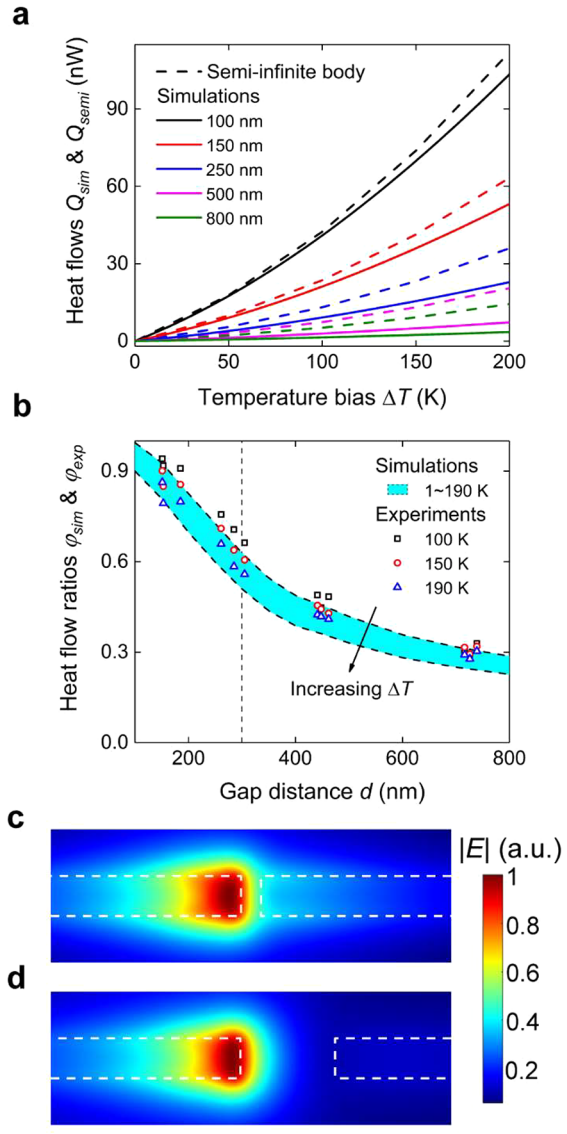

Figure 4. Theoretical analysis by comparing with the semi-infinite body theory. (a) Comparison between the heat flows from semi-infinite body theory (dashed line) and fluctuational-EM simulation (solid line). The near-field radiation heat transfer between the subwavelength membranes is lower than the prediction between semi-infinite bodies. We attribute the lower heat flow across the subwavelength surfaces to the energy carried by the polaritons scattered away from the gap. (b) Heat flow ratio φ_{sim} (shaded region) and φ_{exp} (dots) as a function of gap distance where φ_{sim} and φ_{exp} are the ratios of fluctuational-EM simulation and experimental measurements to semi-infinite body predictions, respectively. φ_{sim} or φ_{exp} dramatically increases from ~20% to almost 100% as the gap distance decreases from 800 to 100 nm. Besides, φ_{sim} or φ_{exp} increases with a higher rate as the gap distance decreases below the thickness, 300 nm. (c,d) Electric field profiles between the parallel membranes with gap distances of 150 and 700 nm, respectively. The electric field profile at the 150 nm gap distance is more uniformly distributed within the separation.

and approaches that between the semi-infinite bodies (e.g., $\varphi_{sim} > 0.5$ for $d < 300$ nm). The increase in φ_{sim} (or φ_{exp}) depends on two main criteria. First, at large separations, the surface phonon polaritons have wavelengths, λ, that are larger than but comparable with t. At shorter separations, the surface phonon polaritons possess smaller wavelengths and interact less with the lateral x and z dimensions (see the Supporting Information for polariton and wavelength relations). As a result, the scattering of these polaritons at shorter gap distances is less pronounced compared with that at larger separations. Figure 4c,d shows the electric field profile around the hot region for separation gaps of 150 and 700 nm, respectively. As seen, the field away from the surface (light blue and cyan regions) is spatially distributed along the thickness because of scattering. However, the field closer to the surface (yellow and green regions) is more uniformly distributed, thereby resembling the semi-infinite bodies (no lateral dependence of the field profile). This behavior leads to the heat transfer rate closer to that between the semi-infinite bodies at shorter distances. Second, the rate of the increase in φ_{sim} (or φ_{exp}) is enhanced for the separations below the thickness of the membrane. Spatial confinement along the z-axis prevents the existence of polaritons with wavelengths larger than thickness t. These polaritons are only supported along the length direction (x-axis) and become the main contributors to energy transport at large separations. At separations less than the thickness t, polaritons with wavelength smaller than thickness mainly transport energy across the gap, and these polaritons exist along both the thickness (z-axis) and the length (x-axis) directions. Thus, at the short separations, the contributing polaritons supported in both directions carry a higher total energy and approach the semi-infinite bodies where polaritons exist in all directions without any spatial constraint.

In this work, we design and fabricate coplanar nanodevices to measure the near-field thermal radiation between subwavelength coplanar membranes. Through high-sensitivity measurements, we accurately quantify the near-field heat flow, which shows excellent agreement with fluctuational electrodynamics simulations. Compared with blackbody radiation, we observe 20-fold enhancement in thermal radiation between the two subwavelength structures with a separation gap of ~150 nm, while the maximum thermal conductance is still much less than these previously reported in near-field experiments because of the small heat exchange area of the subwavelength structure. In addition, our analysis finds that the near-field thermal radiation between the subwavelength coplanar membranes remains lower than that based on the semi-infinite model, which is attributed to energy escaping from the subwavelength confinements due to scattering of polaritons and less contributions from polariton modes with large wavelengths. Our findings elucidate the near-field energy transfer between subwavelength structures, thereby paving the way for the development of coplanar near-field nanodevices for energy harvesting and thermal management.

■ ASSOCIATED CONTENT

Supporting Information

The Supporting Information is available free of charge at https://pubs.acs.org/doi/10.1021/acs.nanolett.3c03748.

Fabrication process, gap distances measurements of the devices, temperature profile on the emitting membrane, near-field thermal emission from the emitting membrane, reference devices, overview of thermal measurement, temperature-resistance calibration of PRT, thermal frequency domain responses of the heater and sensor, determining temperature variations from the platinum thermometer, temperature profile along the sensor beam and calibration of G_s, noise floor of the

https://doi.org/10.1021/acs.nanolett.3c03748
Nano Lett. 2024, 24, 1502−1509

measurement, linear interpolations of raw data, radiation heat flows of all measured devices, radiation heat conductance of all measured devices, near-field enhancements of all measured devices, view factor calculation, dielectric permittivity of silicon nitride, comparison with far-field super-Planckian thermal radiation, reflection measurement of the silicon nitride membrane, semi-infinite body calculation, polariton and wavelength relation, electric field simulation, and the influence of height deviation (PDF)

AUTHOR INFORMATION

Corresponding Author

Sheng Shen − *Department of Mechanical Engineering, Carnegie Mellon University, Pittsburgh, Pennsylvania 15213, United States;* orcid.org/0000-0002-9951-0814; Email: sshen1@cmu.edu

Authors

Xiao Luo − *Department of Mechanical Engineering, Carnegie Mellon University, Pittsburgh, Pennsylvania 15213, United States*

Hakan Salihoglu − *Department of Mechanical Engineering, Carnegie Mellon University, Pittsburgh, Pennsylvania 15213, United States*

Zexiao Wang − *Department of Mechanical Engineering, Carnegie Mellon University, Pittsburgh, Pennsylvania 15213, United States*

Zhuo Li − *Department of Mechanical Engineering, Carnegie Mellon University, Pittsburgh, Pennsylvania 15213, United States*

Hyeonggyun Kim − *Department of Mechanical Engineering, Carnegie Mellon University, Pittsburgh, Pennsylvania 15213, United States*

Xiu Liu − *Department of Mechanical Engineering, Carnegie Mellon University, Pittsburgh, Pennsylvania 15213, United States*

Jiayu Li − *Department of Mechanical Engineering, Carnegie Mellon University, Pittsburgh, Pennsylvania 15213, United States*

Bowen Yu − *Department of Mechanical Engineering, Carnegie Mellon University, Pittsburgh, Pennsylvania 15213, United States*

Shen Du − *Department of Mechanical Engineering, Carnegie Mellon University, Pittsburgh, Pennsylvania 15213, United States*

Complete contact information is available at: https://pubs.acs.org/10.1021/acs.nanolett.3c03748

Author Contributions

‡X.Luo, H.S., Z.W., and Z.L. contributed equally. X.Luo and S.S. conceived the concept of the work. X.Luo, Z.W., B.Y., and S.D. designed the thermal nanodevice. X.Luo, Z.W., H.K., and B.Y. developed the fabrication process. X.Luo measured the gap distance. H.S. measured the height difference. X.Luo, Z.W., and H.S. developed the experimental setup and measurement procedure. X.Luo, Z.L., and J.L. implemented the fluctuational electromagnetic simulations. H.S. developed the analytical calculation of the near-field radiation between semi-infinite bodies. H.K., X.Liu, J.L., B.Y., and S.D. provided additional discussions on the overall ideas. The manuscript was written by X.Luo, H.S., and S.S. with comments and input from all authors. S.S. supervised the research.

Notes

The authors declare no competing financial interest.

During the preparation of this manuscript, S.S. and X.Luo learned that the group of Prof. Chris Dames at UC Berkeley is also preparing a manuscript (arXiv preprint arXiv:2310.20356) on lateral near-field thermal radiation between silicon carbide membranes.

ACKNOWLEDGMENTS

The authors are grateful to the Defense Threat Reduction Agency (Grant No. HDTRA1-19-1-0028) and the National Science Foundation (Grant No. CBET-1931964). X.Luo would like to thank the Neil and Jo Bushnell Fellowship in Engineering. Z.L. would like to thank the Liang Ji-Dian Fellowship. The authors also acknowledge the Claire & John Bertucci Nanotechnology Laboratory at Carnegie Mellon University (BNL-78657879) for the fabrication of the devices and the Material Characterization Facility at Carnegie Mellon University (MCF-677785) for scanning electron microscopy.

REFERENCES

(1) Heinrich, A. J.; Oliver, W. D.; Vandersypen, L. M. K.; Ardavan, A.; Sessoli, R.; Loss, D.; Jayich, A. B.; Fernandez-Rossier, J.; Laucht, A.; Morello, A. Quantum-Coherent Nanoscience. *Nat. Nanotechnol.* **2021**, *16* (12), 1318−1329.

(2) Altug, H.; Oh, S.-H.; Maier, S. A.; Homola, J. Advances and Applications of Nanophotonic Biosensors. *Nat. Nanotechnol.* **2022**, *17* (1), 5−16.

(3) Corato-Zanarella, M.; Gil-Molina, A.; Ji, X.; Shin, M. C.; Mohanty, A.; Lipson, M. Widely Tunable and Narrow-Linewidth Chip-Scale Lasers from near-Ultraviolet to near-Infrared Wavelengths. *Nat. Photonics* **2023**, *17* (2), 157−164.

(4) Thompson, D.; Zhu, L.; Mittapally, R.; Sadat, S.; Xing, Z.; McArdle, P.; Qazilbash, M. M.; Reddy, P.; Meyhofer, E. Hundred-Fold Enhancement in Far-Field Radiative Heat Transfer over the Blackbody Limit. *Nature* **2018**, *561* (7722), 216−221.

(5) Rodriguez, A. W.; Capasso, F.; Johnson, S. G. The Casimir Effect in Microstructured Geometries. *Nat. Photonics* **2011**, *5* (4), 211−221.

(6) Fong, K. Y.; Li, H.-K.; Zhao, R.; Yang, S.; Wang, Y.; Zhang, X. Phonon Heat Transfer across a Vacuum through Quantum Fluctuations. *Nature* **2019**, *576*, 243−247.

(7) Xu, Z.; Gao, X.; Bang, J.; Jacob, Z.; Li, T. Non-Reciprocal Energy Transfer through the Casimir Effect. *Nat. Nanotechnol.* **2022**, *17* (2), 148−152.

(8) St-Gelais, R.; Zhu, L.; Fan, S.; Lipson, M. Near-Field Radiative Heat Transfer between Parallel Structures in the Deep Subwavelength Regime. *Nat. Nanotechnol.* **2016**, *11* (6), 515−519.

(9) Lucchesi, C.; Vaillon, R.; Chapuis, P.-O. Radiative Heat Transfer at the Nanoscale: Experimental Trends and Challenges. *Nanoscale Horizons* **2021**, *6* (3), 201−208.

(10) Song, B.; Fiorino, A.; Meyhofer, E.; Reddy, P. Near-Field Radiative Thermal Transport: From Theory to Experiment. *AIP Adv.* **2015**, *5* (5), No. 053503.

(11) Shen, S.; Narayanaswamy, A.; Chen, G. Surface Phonon Polaritons Mediated Energy Transfer between Nanoscale Gaps. *Nano Lett.* **2009**, *9* (8), 2909−2913.

(12) Zhu, L.; Fiorino, A.; Thompson, D.; Mittapally, R.; Meyhofer, E.; Reddy, P. Near-Field Photonic Cooling through Control of the Chemical Potential of Photons. *Nature* **2019**, *566* (7743), 239−244.

(13) Latella, I.; Biehs, S.-A.; Ben-Abdallah, P. Smart Thermal Management with Near-Field Thermal Radiation. *Opt. Express* **2021**, *29* (16), 24816.

(14) Mittapally, R.; Lee, B.; Zhu, L.; Reihani, A.; Lim, J. W.; Fan, D.; Forrest, S. R.; Reddy, P.; Meyhofer, E. Near-Field Thermophoto-

voltaics for Efficient Heat to Electricity Conversion at High Power Density. *Nat. Commun.* **2021**, *12*, 4364.
(15) Lucchesi, C.; Cakiroglu, D.; Perez, J.-P.; Taliercio, T.; Tournié, E.; Chapuis, P.-O.; Vaillon, R. Near-Field Thermophotovoltaic Conversion with High Electrical Power Density and Cell Efficiency above 14%. *Nano Lett.* **2021**, *21* (11), 4524−4529.
(16) Bhatt, G. R.; Zhao, B.; Roberts, S.; Datta, I.; Mohanty, A.; Lin, T.; Hartmann, J.-M.; St-Gelais, R.; Fan, S.; Lipson, M. Integrated Near-Field Thermo-Photovoltaics for Heat Recycling. *Nat. Commun.* **2020**, *11*, 2545.
(17) Hu, L.; Narayanaswamy, A.; Chen, X.; Chen, G. Near-Field Thermal Radiation between Two Closely Spaced Glass Plates Exceeding Planck's Blackbody Radiation Law. *Appl. Phys. Lett.* **2008**, *92* (13), No. 133106.
(18) Ying, X.; Sabbaghi, P.; Sluder, N.; Wang, L. Super-Planckian Radiative Heat Transfer between Macroscale Surfaces with Vacuum Gaps down to 190 Nm Directly Created by SU-8 Posts and Characterized by Capacitance Method. *ACS Photonics* **2020**, *7* (1), 190−196.
(19) Tang, L.; Desutter, J.; Francoeur, M. Near-Field Radiative Heat Transfer between Dissimilar Materials Mediated by Coupled Surface Phonon- And Plasmon-Polaritons. *ACS Photonics* **2020**, *7* (5), 1304−1311.
(20) Sabbaghi, P.; Long, L.; Ying, X.; Lambert, L.; Taylor, S.; Messner, C.; Wang, L. Super-Planckian Radiative Heat Transfer between Macroscale Metallic Surfaces Due to near-Field and Thin-Film Effects. *J. Appl. Phys.* **2020**, *128* (2), No. 025305.
(21) Yang, J.; Du, W.; Su, Y.; Fu, Y.; Gong, S.; He, S.; Ma, Y. Observing of the Super-Planckian near-Field Thermal Radiation between Graphene Sheets. *Nat. Commun.* **2018**, *9*, 4033.
(22) DeSutter, J.; Tang, L.; Francoeur, M. A Near-Field Radiative Heat Transfer Device. *Nat. Nanotechnol.* **2019**, *14* (8), 751−755.
(23) Lim, M.; Song, J.; Lee, S. S.; Lee, J.; Lee, B. J. Surface-Plasmon-Enhanced Near-Field Radiative Heat Transfer between Planar Surfaces with a Thin-Film Plasmonic Coupler. *Phys. Rev. Appl.* **2020**, *14*, No. 014070.
(24) Shi, K.; Chen, Z.; Xing, Y.; Yang, J.; Xu, X.; Evans, J.-S.; He, S. Near-Field Radiative Heat Transfer Modulation with an Ultrahigh Dynamic Range through Mode Mismatching. *Nano Lett.* **2022**, *22* (19), 7753−7760.
(25) Shi, K.; Chen, Z.; Xu, X.; Evans, J.-S.; He, S. Optimized Colossal Near-Field Thermal Radiation Enabled by Manipulating Coupled Plasmon Polariton Geometry. *Adv. Mater.* **2021**, *33*, No. 2106097.
(26) Lucchesi, C.; Vaillon, R.; Chapuis, P.-O. Temperature Dependence of Near-Field Radiative Heat Transfer above Room Temperature. *Mater. Today Phys.* **2021**, *21*, No. 100562.
(27) Bernardi, M. P.; Milovich, D.; Francoeur, M. Radiative Heat Transfer Exceeding the Blackbody Limit between Macroscale Planar Surfaces Separated by a Nanosize Vacuum Gap. *Nat. Commun.* **2016**, *7*, 12900.
(28) Ghashami, M.; Geng, H.; Kim, T.; Iacopino, N.; Cho, S. K.; Park, K. Precision Measurement of Phonon-Polaritonic Near-Field Energy Transfer between Macroscale Planar Structures under Large Thermal Gradients. *Phys. Rev. Lett.* **2018**, *120* (17), No. 175901.
(29) Giroux, M.; Stephan, M.; Brazeau, M.; Molesky, S.; Rodriguez, A. W.; Krich, J. J.; Hinzer, K.; St-Gelais, R. Measurement of Near-Field Radiative Heat Transfer at Deep Sub-Wavelength Distances Using Nanomechanical Resonators. *Nano Lett.* **2023**, *23* (18), 8490−8497.
(30) Lim, M.; Song, J.; Lee, S. S.; Lee, B. J. Tailoring Near-Field Thermal Radiation between Metallo-Dielectric Multilayers Using Coupled Surface Plasmon Polaritons. *Nat. Commun.* **2018**, *9* (1), 4302.
(31) Song, B.; Thompson, D.; Fiorino, A.; Ganjeh, Y.; Reddy, P.; Meyhofer, E. Radiative Heat Conductances between Dielectric and Metallic Parallel Plates with Nanoscale Gaps. *Nat. Nanotechnol.* **2016**, *11* (6), 509−514.
(32) Song, B.; Ganjeh, Y.; Sadat, S.; Thompson, D.; Fiorino, A.; Fernández-Hurtado, V.; Feist, J.; Garcia-Vidal, F. J.; Cuevas, J. C.; Reddy, P.; Meyhofer, E. Enhancement of Near-Field Radiative Heat Transfer Using Polar Dielectric Thin Films. *Nat. Nanotechnol.* **2015**, *10* (3), 253−258.
(33) Fiorino, A.; Thompson, D.; Zhu, L.; Song, B.; Reddy, P.; Meyhofer, E. Giant Enhancement in Radiative Heat Transfer in Sub-30 Nm Gaps of Plane Parallel Surfaces. *Nano Lett.* **2018**, *18* (6), 3711−3715.
(34) Shi, K.; Sun, Y.; Chen, Z.; He, N.; Bao, F.; Evans, J.; He, S. Colossal Enhancement of Near-Field Thermal Radiation across Hundreds of Nanometers between Millimeter-Scale Plates through Surface Plasmon and Phonon Polaritons Coupling. *Nano Lett.* **2019**, *19* (11), 8082−8088.
(35) Salihoglu, H.; Nam, W.; Traverso, L.; Segovia, M.; Venuthurumilli, P. K.; Liu, W.; Wei, Y.; Li, W.; Xu, X. Near-Field Thermal Radiation between Two Plates with Sub-10 Nm Vacuum Separation. *Nano Lett.* **2020**, *20* (8), 6091−6096.
(36) St-Gelais, R.; Guha, B.; Zhu, L.; Fan, S.; Lipson, M. Demonstration of Strong Near-Field Radiative Heat Transfer between Integrated Nanostructures. *Nano Lett.* **2014**, *14* (12), 6971−6975.
(37) Loomis, J. J.; Maris, H. J. Theory of Heat Transfer by Evanescent Electromagnetic Waves. *Phys. Rev. B* **1994**, *50* (24), 18517−18524.
(38) Joulain, K.; Mulet, J.-P.; Marquier, F.; Carminati, R.; Greffet, J.-J. Surface Electromagnetic Waves Thermally Excited: Radiative Heat Transfer, Coherence Properties and Casimir Forces Revisited in the Near Field. *Surf. Sci. Rep.* **2005**, *57* (3−4), 59−112.
(39) Basu, S.; Yang, Y.; Wang, L. Near-Field Radiative Heat Transfer between Metamaterials Coated with Silicon Carbide Thin Films. *Appl. Phys. Lett.* **2015**, *106* (3), No. 033106.
(40) Boriskina, S. V.; Tong, J. K.; Huang, Y.; Zhou, J.; Chiloyan, V.; Chen, G. Enhancement and Tunability of Near-Field Radiative Heat Transfer Mediated by Surface Plasmon Polaritons in Thin Plasmonic Films. *Photonics* **2015**, *2* (2), 659−683.
(41) Francoeur, M.; Mengüç, M. P.; Vaillon, R. Near-Field Radiative Heat Transfer Enhancement via Surface Phonon Polaritons Coupling in Thin Films. *Appl. Phys. Lett.* **2008**, *93* (4), No. 043109.
(42) Biehs, S.-A.; Rousseau, E.; Greffet, J.-J. Mesoscopic Description of Radiative Heat Transfer at the Nanoscale. *Phys. Rev. Lett.* **2010**, *105* (23), No. 234301.
(43) Wingert, M. C.; Chen, Z. C. Y.; Kwon, S.; Xiang, J.; Chen, R. Ultra-Sensitive Thermal Conductance Measurement of One-Dimensional Nanostructures Enhanced by Differential Bridge. *Rev. Sci. Instrum.* **2012**, *83* (2), No. 024901.
(44) Zheng, J.; Wingert, M. C.; Dechaumphai, E.; Chen, R. Sub-picowatt/kelvin resistive thermometry for probing nanoscale thermal transport. *Rev. Sci. Instrum.* **2013**, *84* (11), No. 114901.
(45) Reid, M. T. H.; Johnson, S. G. Efficient Computation of Power, Force, and Torque in BEM Scattering Calculations. *IEEE Trans. Antennas Propag.* **2015**, *63* (8), 3588−3598.
(46) Rodriguez, A. W.; Reid, M. T. H.; Johnson, S. G. Fluctuating-Surface-Current Formulation of Radiative Heat Transfer: Theory and Applications. *Phys. Rev. B* **2013**, *88* (5), No. 054305.

https://doi.org/10.1021/acs.nanolett.3c03748
Nano Lett. 2024, 24, 1502−1509